Preferential penetration path of gallium into grain boundary in practical aluminium alloy

Kobayashi, Masakazu
Toyohashi University of Technology

Toda, Hiroyuki
Toyohashi University of Technology

Uesugi, kentaro
Japan Synchrotron Radiation Research Institute(JASRI)

Ogaki, Tomomi
Toyohashi University of Technology

他

出版情報：Philosophical Magazine. 86 (28), 2007-02-21. Taylor & Francis
バージョン：
権利関係：

Preferential penetration path of gallium into grain boundary in practical aluminium alloy

Masakazu KOBAYASHI

Department of Production Systems Engineering, Toyohashi University of Technology, 1-1, Hibarigaoka, Tempaku-cho, Toyohashi, Aichi 441-8580 JAPAN.

TEL +81-532-47-0111 (5220), FAX +81-532-44-6690,

E-mail m-kobayashi@sp-Mac4.pse.tut.ac.jp

Hiroyuki TODA

Department of Production Systems Engineering, Toyohashi University of Technology, 1-1, Hibarigaoka, Tempaku-cho, Toyohashi, Aichi 441-8580 JAPAN.

TEL +81-532-47-6697, FAX +81-532-44-6690, E-mail toda@sp-Mac4.pse.tut.ac.jp

Kentaro UESUGI

Japan Synchrotron Radiation Research Institute, 1-1-1, Kouto, Sayo-cho, Sayo-gun, Hyogo 679-5198 JAPAN.

TEL +81-791-58-0803-3928, E-mail ueken@spring8.or.jp

Tomomi OHGAKI

Department of Production Systems Engineering, Toyohashi University of Technology, 1-1, Hibarigaoka, Tempaku-cho, Toyohashi, Aichi 441-8580 JAPAN.

TEL +81-532-47-0111 (5220), FAX +81-532-44-6690,

E-mail ohgaki@sp-Mac4.pse.tut.ac.jp

Toshiro KOBAYASHI

Department of Production Systems Engineering, Toyohashi University of Technology, 1-1, Hibarigaoka, Tempaku-cho, Toyohashi, Aichi 441-8580 JAPAN.

TEL +81-532-47-2001, E-mail r2tk10@edu.cc.tut.ac.jp

Yoshimasa TAKAYAMA

Department of Mechanical Systems Engineering, Utsunomiya University, 7-1-2, Yoto, Utsunomiya, Tochigi 321-8585 JAPAN.

TEL +81-28-689-6033, FAX +81-28-689-6078

E-mail takayama@mech.utsunomiya-u.ac.jp

Byung-Guk AHN

Faculty of Advanced Materials Engineering, Chonbuk National University, Jeonju 561-756 KOREA.

TEL +82-63-270-2300, FAX +82-63-270-2386, E-mail bkahn@chonbuk.ac.kr

Abstract: 176 words

Text: 4928 words

Preferential penetration path of gallium into grain boundary in practical aluminium alloy

M. KOBAYASHI[†], H. TODA[†], K. UESUGI[‡], T. OHGAKI[†],

T. KOBAYASHI[†], Y. TAKAYAMA[¶] and B.-G. AHN[§]

[†]Department of Production Systems Engineering, Toyohashi University of Technology,

Toyohashi Aichi 441-8580, JAPAN.

[‡] Japan Synchrotron Radiation Research Institute, Sayo-cho Hyogo 679-5198, JAPAN.

[¶] Department of Mechanical Systems Engineering, Utsunomiya University,

Utsunomiya Tochigi 321-8585, JAPAN.

[§] Faculty of Advanced Materials Engineering, Chonbuk National University,

Jeonju, 561-756, KOREA.

Abstract

The preferential penetration of a liquid metal along grain boundary in polycrystalline metals is a well-known phenomenon. Gallium decorated GB networks of rolled aluminium alloys have been visualised three-dimensionally using the high-resolution synchrotron radiation computer tomography (SR-CT). The distribution of gallium concentration along GBs is measured in terms of X-ray absorption. Statistically correction for blurring is performed to raise accuracy of the measurement, and then compared with orientation mapping by the SEM/EBSP method on the surface of a tomographic specimen. The pancake-like grain microstructure formed by a rolling process causes the anisotropy of penetration direction. Although the gallium penetrated into high-angle GBs, all of the high-angle GBs are not necessarily decorated by the gallium. The reason for this may be explained by considering geometrically possible penetration paths that seems to be dependent on local grain arrangement and GB structure through each path. The dependence of the gallium concentration on the rotation axis of misorientation has been found along the high-angle GBs. Especially, GB with a specific misorientation (<221> as a misorientation axis) showed high gallium concentration.

Keywords: grain boundary wetting, grain boundary network, synchrotron radiation, computer tomography

1. Introduction

The preferential penetration of a liquid metal along grain boundary (GB) in polycrystalline metals is a well-known phenomenon, which causes brittle fracture called as the Liquid Metal Embrittlement (LME)[1]. Intergranular penetration that causes LME has been observed in Al-Ga, Zn-Ga, Ni-Bi, Cu-Bi systems and etc. LME is a serious matter for structural material because it refers to the instantaneous reduction or loss of ductility of an otherwise ductile material when stressed in contact with liquid metal. The detrimental LME effect for structural materials has been investigated to date. For example, mechanical properties of martensitic steel 91, which is intend to utilize for a cooling system of nuclear reactor, in contact with lead has been reported for various metallurgical and mechanical conditions [2][3]. Fatigue behaviour in mercury environments has been studied for 316LN stainless steel, which is the prime candidate target-container for the spallation neutron source [4]. When metallurgical and mechanical conditions are satisfied, the LME can occur and affect mechanical properties and behaviour.

Its fundamental mechanism has been studied extensively from viewpoints of grain-boundary wetting (GBW) [5], stress driven LME [6], GB diffusivity [7], liquid-solid interface energy [8][9] and so on. Theoretical models have been developed on the basis of thermodynamic and fracture mechanics mechanisms [10][11]. However, it is not still clear which mechanism dominates the penetration behaviour due to complicated GB structure, its nanoscopic size and various possible external and internal variables.

An Al-liquid Ga system has been particularly investigated as a model system. Rapid penetration and subsequent replacement of GB in aluminium alloys by liquid gallium occurs even in the absence of an applied stress. The spontaneous penetration in a stress free condition is considered to be by the GBW. The GBW gives us a thermodynamic equation for driving force, F_w depending on temperature as follows,

$$F_w = \gamma_{GB} - 2\gamma_{SL} > 0, \qquad \text{at } T > T_w, \tag{1}$$

where γ_{GB} is GB energy, γ_{SL} is solid/liquid interface energy and T_w is GBW transition temperature, which is considered to depend on GB structure. The driving force becomes positive

above T_w, by which liquid gallium can penetrate into aluminium GBs.

Channels of liquid gallium formed by the GB penetration have been often observed as crack-like shape that is a few micrometers in the width. Penetration rate at a channel-front through aluminium bicrystal GB was reported to be several few μm/s by Hugo and Hoagland [12][13] and Ludwig et al. [14] by means of the transmission electron microscopy (TEM) and the synchrotron radiation radiography, respectively. The fast penetration observed could not be explained by GB diffusivity, although GB is a high-diffusivity path in polycrystalline materials. According to the TEM observation by Hugo and Hoagland [12], a line defect like a climbing edge dislocation, which produced a stress-field, was found at a moving penetration front. They attributed the fast penetration to a few monolayers that might consist of gallium atoms interacting with an aluminium GB. Ludwig and his co-workers [14] investigated by high-resolution radiography, pointing out that the fast penetration process was controlled by an internal stress, which was as weak as 0.5-0.6MPa, rather than thermodynamic wetting. In a polycrystalline aluminium, internal or residual stress seems to play especially important roles to determine penetration rate through each individual GB, thereby preferential penetration routes are selected because the movement of neighbouring grains are restricted each other.

On the other hand, GB structure, which describes geometrical degrees of freedom and atomic structure, has an influence on physical properties of a polycrystalline material [15][16]. The dependence of GB energy on misorientation and atom arrangement is fairly well known and has been reviewed [17][18][19]. The structure dependence of GB diffusivity was also reported for aluminium GB using germanium radiotracer [20]. Difference in the GBW behaviours has been often utilized to specify GB character in systems of Zn-Ga [21], Fe-Mn-Cu [22][21] and so on, because equation (1) provides a relation between the GBW and the GB energy. In an Al-Ga system, it has been reported that small additions of gallium drastically enhance GB mobility in an aluminium [24]. This result could not be explained by the classical impurity drag effect. The result may suggest a possible influence of gallium addition on GB structure. Thomson et al. calculated the interaction of gallium atoms on a symmetric tilt GB in aluminium and discussed

the possibility of the mobility enhancement and the monolayer presence [25]. They showed gallium atoms attracted to the GB of the aluminium might affect the characteristics and nature of the GB region. If there exists an interaction between two planes that consist of GB and penetrated gallium depending on the structure of the GB plane, the GB structure has any contribution on behaviours.

In this study, preferential penetration path associated with GB structure is investigated in an aluminium alloy by applying gallium using the high-resolution synchrotron radiation computer tomography (SR-CT). Three-dimensional GB networks are visualised by decorating GBs with gallium. The combination of the SR-CT and the GBW seems to provide a powerful tool to get three-dimensional information on GBs in polycrystalline materials [26][27]. Distribution of gallium concentration, which is estimated by X-ray absorption in tomographic data, are compared with an orientation mapping obtained by scanning electron microscope / electron backscattered diffraction pattern (SEM/EBSP) analysis on a sample surface.

2. Experimental methods

2.1. *Sample preparation*

A rolled 6061-alloy plate with a thickness of 20mm was used in this study. The plate was tempered to T6 peak aging by solution heat treatment at 813K for 7.2ks, cooled water quenching after solution heat treatment and aging treatment at 453K for 28.8ks. The chemical compositions of the alloy are listed in Table 1. Samples with an almost squared cross-section of $(0.6mm)^2$ and a length of about 10mm were carefully machined by micro-saw from the central part of plate so that entire cross-section of the sample can be irradiated using the present high-resolution X-ray tomography set-up. Before a liquid gallium was applied onto a specimen surface, some of the samples had been electro-polished by a solution of $HClO_4$: ethanol = 1:8 at 7V at 283K for 420s and then the grain orientation analysis by a SEM/EBSP system was performed. The EBSP scanning for the orientation mapping was preformed on the longitudinal surface of the A6061 aluminium alloy samples in the area of 300×160 μm^2 at a scanning step size of 1.5μm.

Sample and gallium were heated separately at 323K by a hot plate beforehand. A liquid gallium was applied except the surface that has been analysed by the EBSP in advance, then the sample surface was scratched mechanically using tweezers in order to break surface oxide films, enabling direct contact between an aluminium and gallium. After application of gallium, the sample was kept at 323K for 500s on a hot plate to promote the penetration and diffusion of gallium into the aluminium. Air-cooling was used to cool the sample because of small specimen size and high thermal conductivity of aluminium alloy. Surplus gallium on the surface was removed with an adhesive tape. The sample was immediately transferred on to a specimen holder on a high-precise rotation sampling stage for the tomography. A tomographic scan was started about 20min on average after the setting, including the alignment of sample position.

2.2. *High-resolution X-ray CT*

Recent progress in the synchrotron X-ray CT has readily enabled material science-related applications such as the observation of microstructure and deformation mechanism in structural materials [28][29]. The spatial resolution of the SR-CT has been improved significantly owing to the development of optical instruments, providing three-dimensional volume images with sub-micron voxel size.

High-resolution tomographic experiments have been carried out on the beamline BL47XU at the Japanese third-generation synchrotron radiation facility (SPring-8) in Hyogo. Figure 1 shows a schematic illustration of the SR-CT setup used in this study. A monochromatic X-ray beam having a photon energy of 20 keV from a sealed vacuum undulator was used for the experiments. The specimen was located at approximately 49m from the X-ray source. 1500 radiographs were captured by rotating the sample at an increment of 0.12 degree using a Lu_2SiO_5:Ce scintillator. A cooled 4000×2624 element CCD detector (Hamamatsu photonics K.K C4880-41S) was used with a binning mode (1×1). The field of view was 948×626 μm^2. A distance between the sample and the detector was adjusted to be 10mm or 50mm, enhancing (at 50mm) and suppressing (at 10mm) the phase contrast in addition to the conventional absorption

contrast depending on the purpose of the subsequent analysis. The set of radiographs were then reconstructed by means of the convolution integration algorithm. An isotropic voxel with a cutting edge of 0.474 μm was achieved by the present set up.

3. Experimental results

3.1. *Reconstructed volume images*

Three-dimensional reconstructed volume of the rolled 6061 alloy, in which GBs are decorated by the gallium, is shown in figure 2. A half of the aluminium matrix has been removed in order to visualise GB network. Pancake-like GB networks are observed which has been formed during the rolling process. The y-axis indicated in figure 2 corresponds to the rolling direction of the production process. A mean interval of GBs decorated by the gallium was found to be approximately 27μm in perpendicular to the rolling direction. The grain size of approximately 10μm was measured in the same direction by means of the EBSP orientation mapping, indicating that not all the GBs are decorated by the gallium. This means that only preferential penetration paths are visualised at the present combination of the penetration time and temperature conditions. A fraction of GB penetrated at this stage was about 1/3 of all the GBs.

Figure 3 shows a virtual tomographic slice on a X-Y plane specified in figure 2. Complex gallium penetration paths are observed by tortuous white lines that correspond to high X-ray absorption gallium layer along GBs. Some of the white dots are micro-pores filled with gallium, which locate on GBs. Apparently the thickness of the gallium layer seems to be larger in the lower side than that in the upper side where gallium has been applied. There are several possible reasons for this; for example complex penetration paths that can course apparently discontinuous penetration is observed on a specific slice, or the effect of in homogeneous distribution of external parameters such as temperature gradient and internal stress.

Figure 4 indicates distribution of linear absorption coefficient (LAC). The distributions in aluminium matrix are measured by measuring CT volumes before and after gallium penetration. The distribution of gallium is obtained by measuring a part of surplus gallium on

the surface. Peak values of distribution in the aluminium matrix before and after application of gallium are 0.90 and 1.18 mm^{-1}. A peak value of distribution in the gallium is 18.83 mm^{-1}. The distribution in aluminium matrix moves toward the large LAC value side after application of gallium.

Comparison between the reconstructed CT volume and the orientation map obtained by SEM/EBSP analysis is shown in figure 5 to show the correspondence between the gallium distribution and the locations of GBs in an identical surface area. The regions enriched with gallium are highlighted in white in the tomographic image (figure 5 (a)). The EBSP map in figure 5 (b) exhibits grain orientations in colours that correspond to the attached coloured inverse pole figure on normal direction of sheets. Note that black regions shown in the map indicate those where valid grain orientation measurement was not possible probably due to poor polishing of the sample surface. Liquid gallium penetrated in the direction perpendicular to the surface shown. The gallium was applied to the opposite surface and it reached the surface shown in this figure after penetrating through the specimen. Particularly thick gallium layers are observed along some GBs. It has been clarified that gallium is apt to penetrate into high-angle GBs which has misorientation angles larger than 15 degree. No penetration seems to be observed at low-angle GBs (i.e. misorientation angle bellow 15 degree).

3.2. *Gallium concentration profiles*

Figure 6 shows (a) contour map of LAC superposed on a virtual tomographic slice and (b) gallium concentration profiles across GBs H~L specified in (a). The gallium concentration has been calculated from the X-ray absorption data. Note that the gallium concentration profiles contain the strong effect of blurring due to various factors such as time dependent drift of sample or the detector system during scanning. Therefore, the concentration is expressed as apparent one at this stage. The gallium concentration was calculated using the tomographic volume captured without phase contrast, while the slice image was captured with phase contrast to improve image clarify. A set of black and white fringes along interface formed by the phase

contrast imaging inevitably causes inaccurate estimation in chemical composition. Since a mass concentration of gallium, C_{Ga} is in proportion to LAC value, the gallium concentration, C_{Ga} is given as follows:

$$C_{Ga} = (L - \bar{L}_{Al})/(\bar{L}_{Ga} - \bar{L}_{Al}), \quad (2)$$

where L is a LAC value reconstructed in the tomographic volume, $\bar{L}_{Ga}$ and $\bar{L}_{Al}$ are those for pure gallium and pure aluminium, respectively. In this study, $\bar{L}_{Al}$ is used as the peak value of the LAC distribution in the aluminium matrix. The maximum value of the LAC distribution in the gallium corresponds to surplus gallium on the surface, which can be assumed to be almost pure gallium. Therefore using the peak as $\bar{L}_{Ga}$ can be validated on the basis of this assumption. Figure 6 (b) represents the apparent profiles of gallium concentration along intersections across GBs specified in figure 6 (a). The peaks of each profile were identified to locate just on the GBs. The maximum gallium concentration and the shape of the distribution profile vary relatively widely. The maximum and the minimum concentrations are 20.1% and 9.2% on the GBs at points L and J, respectively. The profile at point K shows the broadest distribution. It can be inferred that the higher the peak, the narrower the distribution.

The distribution profiles of gallium concentration across the GBs appear to be broader than that reported by Pereoro-López et al. using X-ray radiography for a polycrystalline pure aluminium [30]. This is partly because of the reasons described earlier on. The Simple correction was performed in order to obtain realistic distribution profiles. By expressing the image blurring with a probability density function, $P(\delta)$, the apparent gallium concentration, $C^{P}_{Ga}(x)$, can be correlated to true concentration, C_{Ga}.

$$C^{p}_{Ga}(x) = \int_{-d_{max}}^{d_{max}} P(\delta) C_{Ga}(x-\delta) d\delta, \quad (3)$$

where x is a distance from a GB position and d_{max} is a half of the maximum width of the deviation. C_{Ga} is simply given as the solution of one-dimensional non-steady state diffusion equation from a GB towards grain interior with an assumption of a constant G_{GB} with time as follows,

$$C_{Ga}(x,t) = C_{GB}\left\{1 - \mathrm{erf}\left(x/\sqrt{4D_{Ga}t}\right)\right\}, \quad (4)$$

where D_{Ga} is the diffusion coefficient of the gallium in the aluminium and the erf is the error function. The calculation to obtain the true distribution profile requires the measurement of d_{max}, Since the image blurring also cause the partial volume effect at an aluminium/air interface, d_{max} can be directly measured by measuring grey value transition at the interface. Figure 7 shows the edge response at the interface between the aluminium and air. It should be mentioned again that only the absorption contrast is utilized to measure the profile in figure 7. The width of the transition region was found to be 2 μm. d_{max} is assumed to be 1 μm in this study.

3.3. *Dependence of gallium concentration on grain boundary character*

The corrected gallium concentration is listed in Table 2 for each GB specified in figure 5 together with GB misorientation angle and rotation axis measured by means of the EBSP technique. Data points assigned above 0.1 of Confidence Index (CI) by the EBSP analysis system were adopted as reliable ones. A β-fibre texture, which generally had formed by rolling in aluminium alloys [31], was found in the sample. Most of the grains belonged to (123)<634> or (110)<112> texture components. Therefore, not only the misorientation angles of 19.5°, 39.1°, 49.3° and 54.0° for high-angle GB but also those of 38.5° and 60.0° for coincidence lattice site grain boundary (CSL-GB) of Σ7 and Σ3 are identified to exist. The misorientations listed in the Table 2 seem to coincide with those predicted above. The maximum concentration of 26.0% is measured along GB D-D' with a rotation of 52.9° about a <552> axis. The minimum of 12.2% is found along GB A-A' with a rotation of 55.3° about a <221> axis. GB G-G' with 15.7% gallium concentration has a Σ3 CSL relation that is characterized by a 60 degree rotation around an <111> axis. No penetration was found through Σ7 GBs within the present measurement. Figure 8 shows gallium concentration as a function of misorientation angle. Only data points with high reliability were plotted in the figure. The GBs with high misorientation angles appear to exhibit relatively high gallium concentration. However, higher misorientation angle do not necessarily

results in higher gallium concentration.

Figure 9 shows distributions of gallium concentration before and after the correction across the GBs specified in figure 5. The misorientation axis, angle and two GB planes orientation are also represented in the figure. Note that the Miller index of GB planes are estimated by assuming a GB plane parallel to the rolling direction, because a scanning step size by the SEM/EBSP was insufficient to determine the GB direction accurately. It can be noticed that distribution profiles are different between the left and right sides with a GB as a centre. Investigating intersection angles formed by the surface and GB at each of the measured point A-A'~G-G' revealed that GB slightly deviated from the right angle. However, the deviation angles ranging from −0.4 to +1.2 degrees were small. A measurement error caused by them (0.085μm was estimated) was smaller than the edge length of a voxel (0.474μm). The concentration profiles would be almost unaffected. The differences between the left and right sides seem to be caused by unlike GB plane structure. The correction was performed separately on the right and left sides. The corrected concentrations show narrower distributions with higher peaks than the apparent ones before the correction. In figure 9 (a), the difference in slopes between the left and right sides are obvious. GB A-A' that has a large misorientation angle of 55.3 degree consists of two different planes of (211) and (843). When GB consists of a pair of (211) plane as shown in figure 9 (c) and (d), the concentration seems to distribute broadly and symmetrically. Figure 9 (d) shows a lower peak value than figure 9 (c) although both of the GBs have a pair of (211) planes. In the case of figure 9 (b), the concentration shows a sharp and symmetrical distribution while the GB possesses two different GB plane.

Changes in gallium concentration along the GB that intersects line D-D' and E-E' in figure 5 are shown in figure 10. A stereoscopic distribution of apparent gallium concentration and a peak value of corrected gallium concentration are shown in figure 10 (a) and (b). Misorientation angle and rotation axis are also included in figure 10 (b). Sudden changes in concentration are observed at y=31.2 and 33.8 μm in the figure, which correspond to the locations of triple GB junction. The present GB separates two different gain pairs misorientation.

The grain pairs 1 and 2 indicated in the figure show misorientation angle of 52 degree and 34 degree on average, respectively. The GB misorientation for grain pair 2 increases gradually with the increase in *y* value. The peak gallium concentration varies between 20 and 60%. The degree of the variation for the grain pair 1 is larger than that for grain pair 2. It is found that parts of the GB rotated about a <221> axis demonstrate relatively high concentration for grain pair 1. However, any considerable effect of the <221>-rotation axis relation concentration is observable for grain pair 2.

4. Discussions

In generally, high-angle GBs that have high-index planes on the interface plane would be expected to provide preferential diffusion or penetration paths for penetrating gallium. Existence of preferential penetration paths has been confirmed in the polycrystalline 6061 aluminium alloy in this study. The penetration paths were formed in parallel to X-Z plane as shown in figure 2. The anisotropic development of penetration direction was caused by the pancake-like grain microstructure formed by rolling. It is also note worthy that all of the high-angle GBs are not necessarily decorated by the gallium. A fraction of GB penetrated by gallium was about 1/3 of all the GBs. The reason for this may be explained by considering geometrically possible penetration paths that seems to be dependent on local grain arrangement and GB structure through each path. Micro-pores filled with gallium were also observed in this study as shown in figure 3, while not all the micro-pores were found close to gallium penetration layers. It has been reported that micro-pores distributed on GBs has been filled with liquid gallium during penetration process in 2024 aluminium alloy [32]. It is suggested that there are thin invisible gallium-penetration-layers which connect with the micro-pore and the gallium on surface, because peak value of LAC distribution in aluminium matrix, which was obtained from the invisible region of gallium penetration layers, has been shifted slightly toward the higher side after the gallium application as shown in figure 4. Change in the LAC was equivalent to gallium concentration of 1.56%.

Dependence of gallium concentration on GB structure has been obtained for the GBs encountered in this study. No penetration was observed in low-angle GBs, which were characterized by misorientation angle below 15 degree. This corresponds well with the assumption that low-angle GBs have low energy. The gallium concentration in high-angle GB varies with not only misorientation angle but also rotation axis of misorientation. Only the information on the misorientation angle was not enough to provide valuable information for the penetration behaviour for high-angle GB. Hugo and Hoagland [13] reported that the GB energy and excess volume that reflect GB structure and which produced by atomistic computer models were not found to correlate with gallium penetration speeds. In the case of gallium concentration, however, the concentrations along GBs were seemed to depend on the rotation axis of misorientation, which should responds to the change of GB planes, as shown in figure 10. The gallium concentration might be sensitive to GB plane orientation. In figure 9, Non-symmetric profile of gallium concentration distribution across GB was observed. Such non-symmetric profile of concentration distribution near GB has also been reported in the case of the diffusion-induced GB migration (DIGM) in zinc diffusion into pure aluminium [33]. In the observation of present study, it was found that the DIGM did not occur because the location of GBs before the application of gallium was investigated by EBSP mapping. It may be possible that the gallium diffuses from the layer along a GB toward grain interior. Difference of diffusivity on GB plane may lead to the non-symmetric profiles. A typical thickness of well-penetrated layers was found to be approximately ~2μm from widths of the concentration profiles shown in figure 9. The thickness value obtained in this study is almost identical to that of the previous study [32] that was also determined using CT. Although gallium layer less than a hundred nanometres in thickness has been reported using the synchrotron radiation radiography [30] in a polycrystalline pure aluminium. It is impossible to detect gallium layers thinner than the present voxel size, i.e. $(0.474\mu m)^3$. Probably, the thin gallium layers have developed from the gallium-applied surface as mentioned above.

The G-G' GB shown in figure 5 has a CSL relation of Σ3. The CSL GBs are generally

regarded to have a low energy and a low diffusivity due to periodic fit of atomistic lattice, although they belong to the high-angle GBs with large misorientation. It can be inferred that the penetration of gallium into those GBs may be difficult. However, high gallium concentration, which was equivalent to random GB (non-CSL GB), was observed at G-G' GB with Σ3 CSL relationship as shown in Table 2. It can be attributed to a large misorientation deviation from an ideal relationship of Σ3 CSL. This may be concerned with reported tendency that GB diffusivity is very sensitive to the misorientation deviation [20]. The misorientation deviation angle of the G-G' Σ3-GB was identified to be 5.3 degree. Although it satisfies the criterion of Brandon for recognizing CSL GBs [34], it seems to be large misorientation. In addition, it is known that the structure of GB planes affect GB character not only in random GBs but also in CSL-GBs. The G-G' Σ3-GB consisting of (211) planes as shown in figure 9 (d) has a high GB energy in comparison with that consisting of (111) planes [16]. If GBs have critical CSL relationship and dense planes on the interface, gallium would not penetrate easily into the GBs. In actually, the existence of such conclusive GBs is probably a rare even in the aluminium alloy with a rolling texture as used in this study. The CSL GB would not have a sufficient influence on the penetration paths of gallium.

5. Conclusions

Three-dimensional GB network of aluminium alloys have been visualised by applying gallium using high-resolution SR-CT. The gallium concentration and its distribution on GBs were measured by analyzing LAC values in the tomographic volumes. The distribution profiles of gallium concentration across GBs were compared with various parameters of GB structure, such as misorientation angle, axis and GB planes, which had been investigated by the SEM/EBSP method on the specimen surface. The results can be summarized as follows:

1. Preferential path of gallium penetration into GBs has been identified. The pancake-like grain microstructure formed by a rolling process causes the anisotropy of penetration

direction. No penetration was observed in low-angle GBs. All of the high-angle GBs are not necessarily decorated by the gallium. Geometrically possible penetration paths seem to be dependent on local grain arrangement and GB structure through each path.

2. The concentration of gallium across GBs was analysed by statistically correcting image blurring. The differences of the gallium concentration profiles on the left and the right sides have been clarified. The gallium concentrations along GBs were seemed to depend on the rotation axis of misorientation. In the high-angle GB with a misorientation angle of approximately 52 degrees, a part of rotated about a <221> axis demonstrated relatively high gallium concentrations.

Acknowledgements

The SR experiment was performed with the approval of JASRI through proposal numbers 2004B0457-NI-np. The authors would like to thank Dr. W. Ludwing for a fruitful discussion and also Mr. H. Makino for an experimental collaboration. We also would like to acknowledge support by the Grant-in-aid for Scientific Research from the Japan Society for the Promotion of Science under Contract No. 15560606 and 17360340.

References

[1] C. F. Old, J. Nucl. Mater. **92** 2 (1980).

[2] A. Legris, G. Nicaise, J. -B. Vogt, J. Foct, D. Gorse and D. Vançon, Scripta metal. **43** 997 (2000).

[3] G. Nicaise, A. Legris, J. B. Vogt, J. Foct, J. Nucl. Mater. **296** 256 (2001).

[4] H. Tian, P. K. Liaw, J. P. Strizak, L. K. Mansur, J. Nucl. Mater. **318** 157 (2003).

[5] E. E. Glickman and M. Nathan, J. Appl. Phys. **85** 3185 (1999).

[6] B. A. Benson and R. G. Hoagland, Scripta metal. **23** 1943 (1989).

[7] M. Lohmann, S. V. Divinski, C. Herzig, Z. Metallkd. **96** 352 (2005).

[8] D. Chatain, E. Rabkin, J. Derenne and J. Bernardini, Acta mater. **49** 1123 (2001).

[9] A. Legris, G. Nicaise, J. -B. Vogt, J. Foct, J. Nucl. Mater. **301** 70 (2002).

[10] P. J. Desré, Scripta Mater. **37** 875 (1997).

[11] E. Rabkin, Scripta Mater. **39** 685 (1998).

[12] R. C. Hugo and R. G. Hoagland, Scripta mater. **41** 1341 (1999).

[13] R. C. Hugo and R. G. Hoagland, Acta mater. **28** 1949 (2000).

[14] W. Ludwig, E. Pereiro-López, D. Bellet, Acta mater. **53** 151 (2005).

[15] V. Randle, Acta mater. **46** 1459 (1997).

[16] P. Davies and V. Randle, Mater. Sci. Technol. **17** 615 (2001).

[17] D. Wolf, Acta metall. **37** 1983 (1989).

[18] D. Wolf, Acta metall. **37** 2823 (1989).

[19] D. Wolf, Acta metall. **38** 781 (1990).

[20] T. Surholt, D. A. Molodov and Chr. Herzig, Acta mater. **46** 5345 (1998).

[21] P. Volovitch, V. Traskine, T. Baudin, L.Barrallier, Interface Science **10** 303 (2002).

[22] M. Takashima, P. Wynblatt and B. L. Adams, Interface science **8** 351 (2000).

[23] P. Wynblatt, M. Takashima, Interface Science **9** 265 (2001).

[24] D. A. Molodov, U. Cyubayko, G. Gottstein, L. S. Shvindlerman, B. Straumal and W. Gust, Phil. Mag. Lett. **72** 361 (1995).

[25] D. I. Thomson, V. Heine, M. C. Payne, N. Marzari and M. W. Finnis, Acta mater. **48** 3623 (2000).

[26] W.Ludwig, S.F. Nielsen, H.F.Poulsen and D. Bellet, Defect and Diffusion Forum, **194-199** 1319 (2001).

[27] K.H.Khor, H.Toda, J.-Y.Buffiére, W.Ludwig, H.S.Ubhi, P.J.Gregson, I.Sinclair, J. phys., Condens. matter **16** S3511 (2004).

[28] J. Baruchel, J.-Y. Buffiére, E. Maire, P. Merle, G. Peix, *X-Ray Tomography in Material Science* (HERMES Science Publications, Paris, 2000)

[29] H. Toda, I. Sinclair, J.-Y. Buffière, E. Maire, T. Connolley, M. Joyce, K. H. Khor, P. Gregson, Phil. Mag. **83** 2429 (2003).

[30] E. Pereiro-López, W. Ludwig, D. Bellet, Acta mater. **52** 321 (2004).

[31] J. Hirsch and K. Lücke, Acta metall. **36** 2863 (1988).

[32] T. Ohgaki, H. Toda, I. Sinclair, J. -Y. Buffière, W. Ludwig, T. Kobayashi, M. Niinomi, T. Akahori, Mater. Sci. Eng. **A406** 261 (2005).

[33] P. Klugkist, A. N. Aleshin, W. Lojkowski, L. S. Shindlerman, W. Gust and E. J. Mittemeijer, Acta mater. **49** 2941 (2001).

[34] D. G. Brandon, Acta metall. **14** 1479 (1966).

Table 1 Chemical compositions of an aluminium used. mass%

	Si	Mg	Ti	Fe	Cu	Zn	Al
A6061 aluminium alloy	0.61	0.98	0.01	0.18	0.35	0.01	Bal.

Table 2 Corrected gallium concentration and misorientation profiles for each GB specified in figure 5.

GB	Concentration (%)	Rotation axis	Misorientation angle (°)
A-A'	12.2	<221>	55.3
B-B'	23.4	<870>	55.4
C-C'	15.5	<321>	33.2
D-D'	26.0	<552>	52.9
E-E'	14.4	<764>	30.3
F-F'	10.8	<433>	55.5
G-G'	15.7	<111>	59.7

Figure 1 Schematic illustration of the synchrotron radiation computer tomography (SR-CT) setup at the BL47XU in the SPring-8.

Figure 2 Three-dimensional reconstructed volume of the rolled 6061 alloy, in which grain boundary (GB) is decorated by gallium. Matrix aluminium has been removed from the half of the volume to visualise the GB network.

Figure 3 A virtual slice of the tomographic volume representing gallium distribution (white in this figure) on a X-Y plane (the axis on specified in Fig. 2).

Figure 4 Distribution of linear absorption coefficient (LAC). Peak values of the LAC distribution in an aluminium matrix, an aluminium matrix after gallium penetration and a gallium are 0.90, 1.18 and 18.83 mm^{-1}, respectively.

Figure 5 Comparison between (a) the reconstructed CT volume and (b) an inverse pole figure map obtained by the SEM/EBSP, representing or corresponding identical surface area. Only high gallium concentration regions are mainly visualised in white.

Figure 6 (a) Contour map of liner absorption coefficient superposed on a virtual tomographic slice. (b) shows gallium concentration profiles across the GBs H~L specified in (a). The gallium concentration has been calculated from the X-ray absorption data.

Figure 7 LAC value transition at the aluminium/air interface.

Figure 8 Corrected gallium concentration as function of misorientation angle.

Figure 9 Apparent and corrected profiles of gallium concentration across GBs specified in Fig. 5. Parameters which represent GB structures are included.

Figure 10 Changes in gallium concentration along GB, (a) corrected gallium concentration along the specific GB specified in Fig. 5 and (b) the variation of misorientation along and rotation axis along the same GB together with the gallium concentration variation.

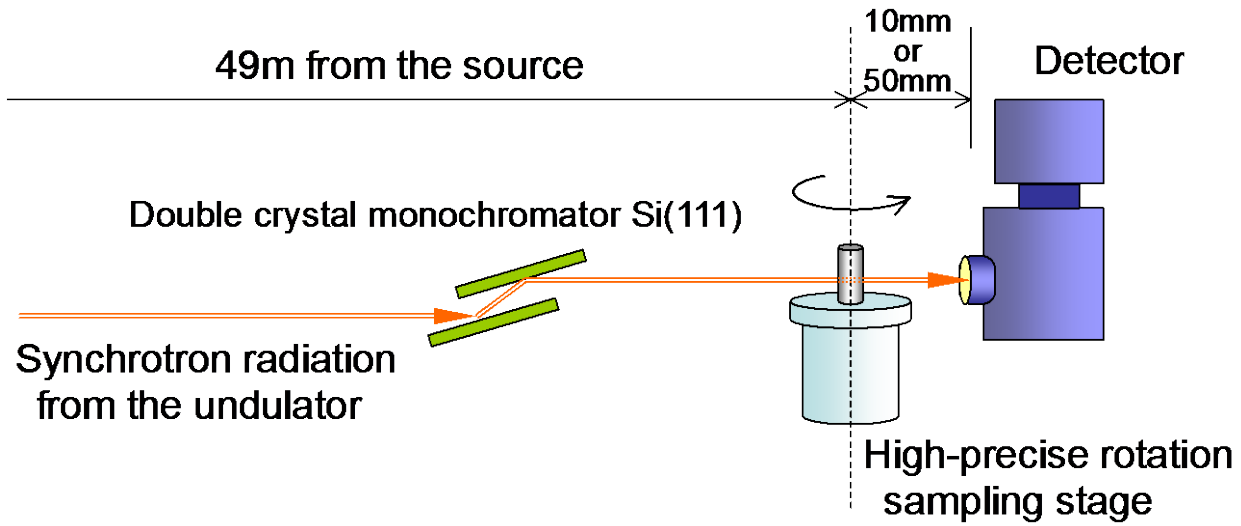

Figure 1 Schematic illustration of the synchrotron radiation computer tomography (SR-CT) setup at the BL47XU in the SPring-8.

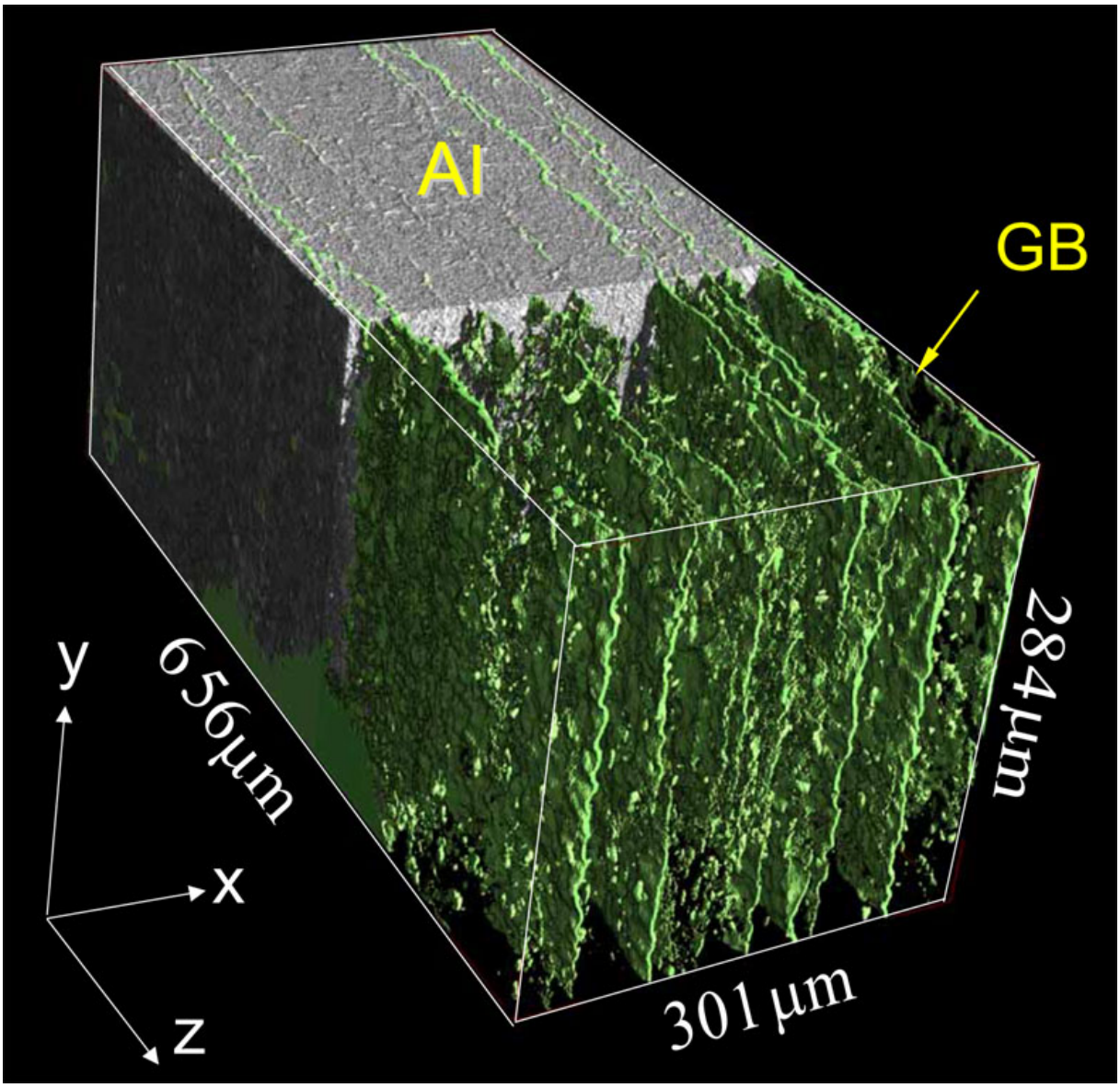

Figure 2 Three-dimensional reconstructed volume of the rolled 6061 alloy, in which grain boundary (GB) is decorated by gallium. Matrix aluminium has been removed from the half of the volume to visualise the GB network.

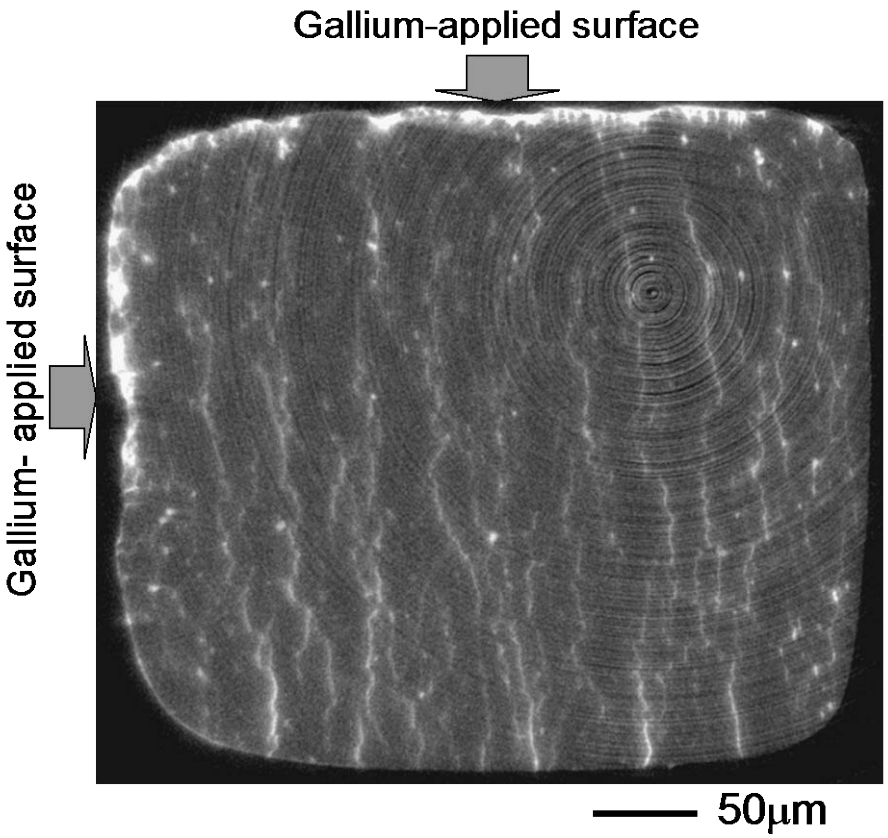

Figure 3 A virtual slice of the tomographic volume representing gallium distribution (white in this figure) on a X-Y plane (the axis on specified in Fig. 2).

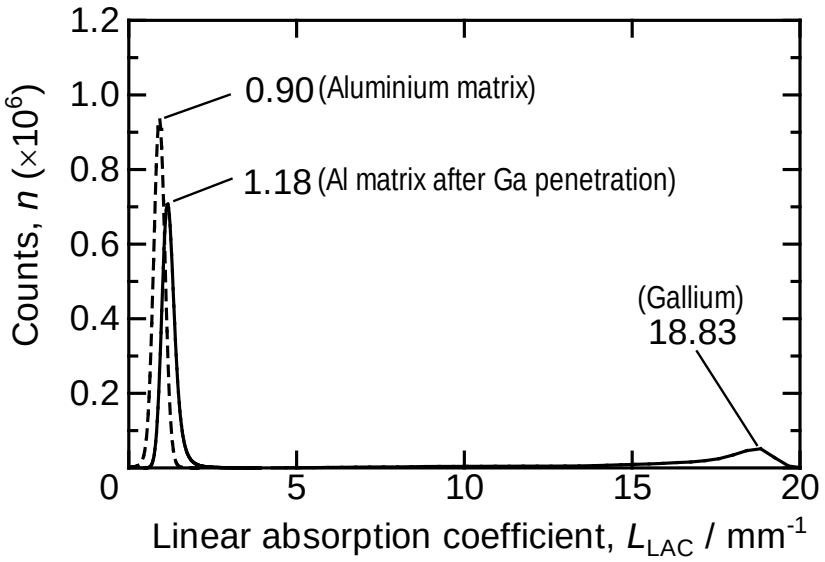

Figure 4 Distribution of linear absorption coefficient (LAC). Peak values of the LAC distribution in an aluminium matrix, an aluminium matrix after gallium penetration and a gallium are 0.90, 1.18 and 18.83 mm^{-1}, respectively.

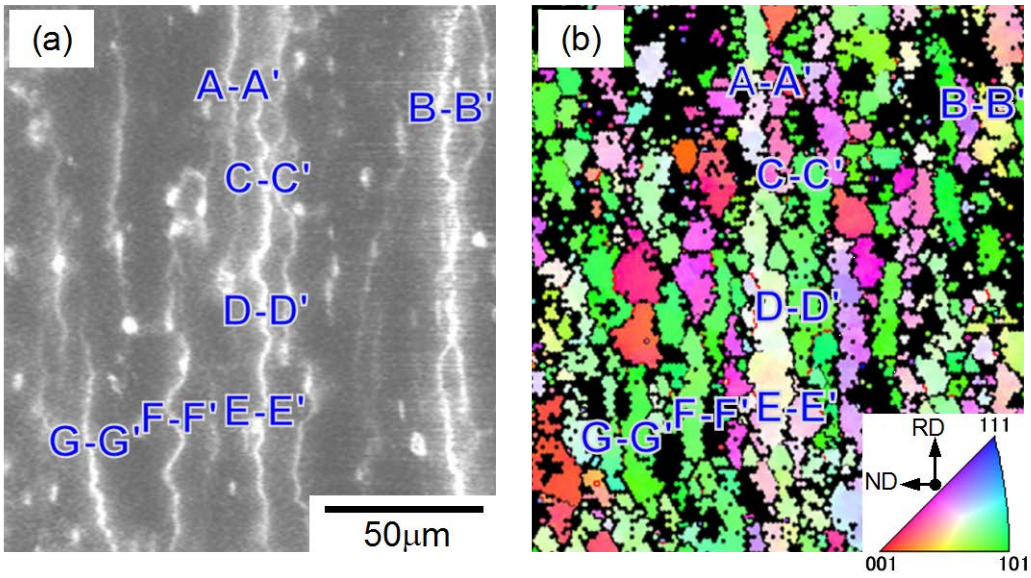

Figure 5 Comparison between (a) the reconstructed CT volume and (b) an inverse pole figure map obtained by the SEM/EBSP, representing or corresponding identical surface area. Only high gallium concentration regions are mainly visualised in white.

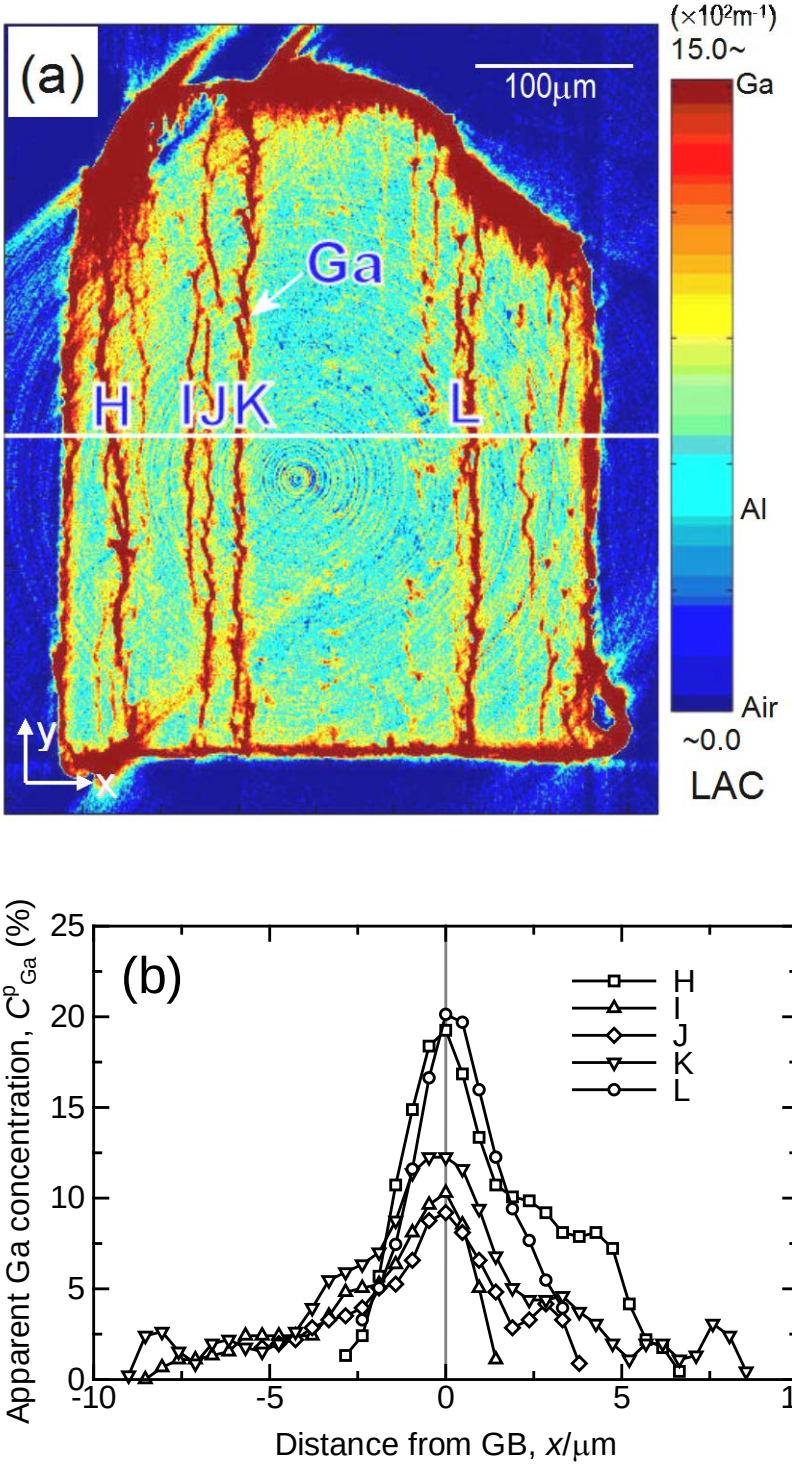

Figure 6 (a) Contour map of liner absorption coefficient superposed on a virtual tomographic slice. (b) shows gallium concentration profiles across the GBs H~L specified in (a). The gallium concentration has been calculated from the X-ray absorption data.

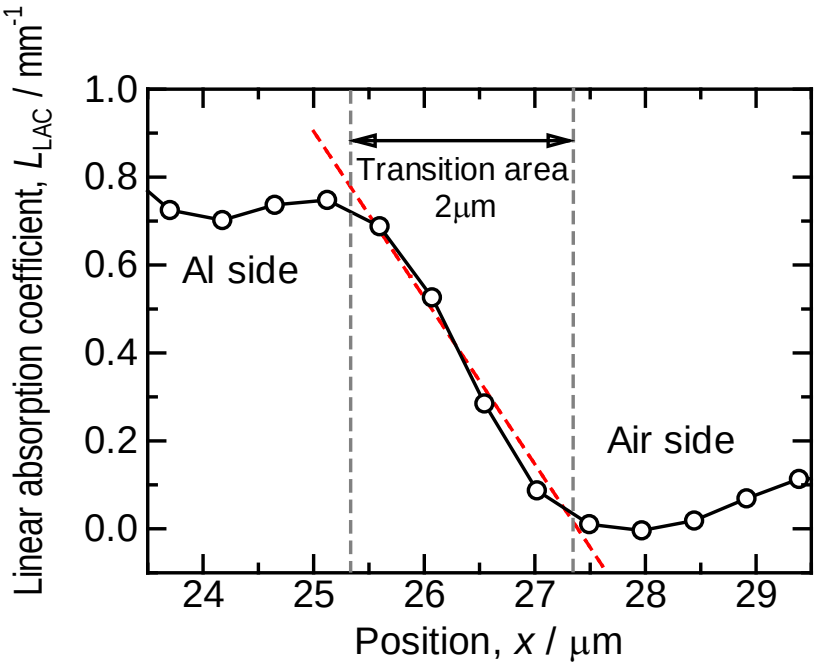

Figure 7 LAC value transition at the aluminium/air interface.

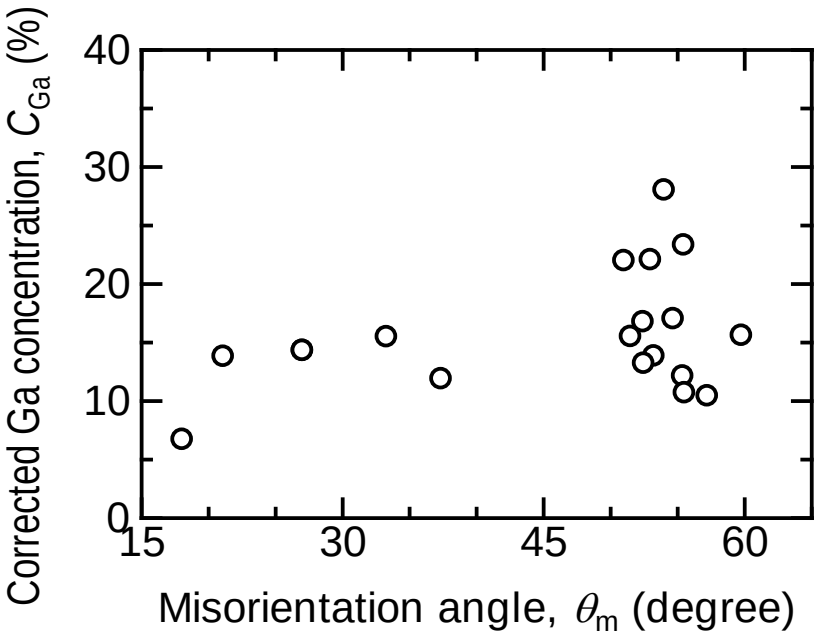

Figure 8 Corrected gallium concentration as function of misorientation angle.

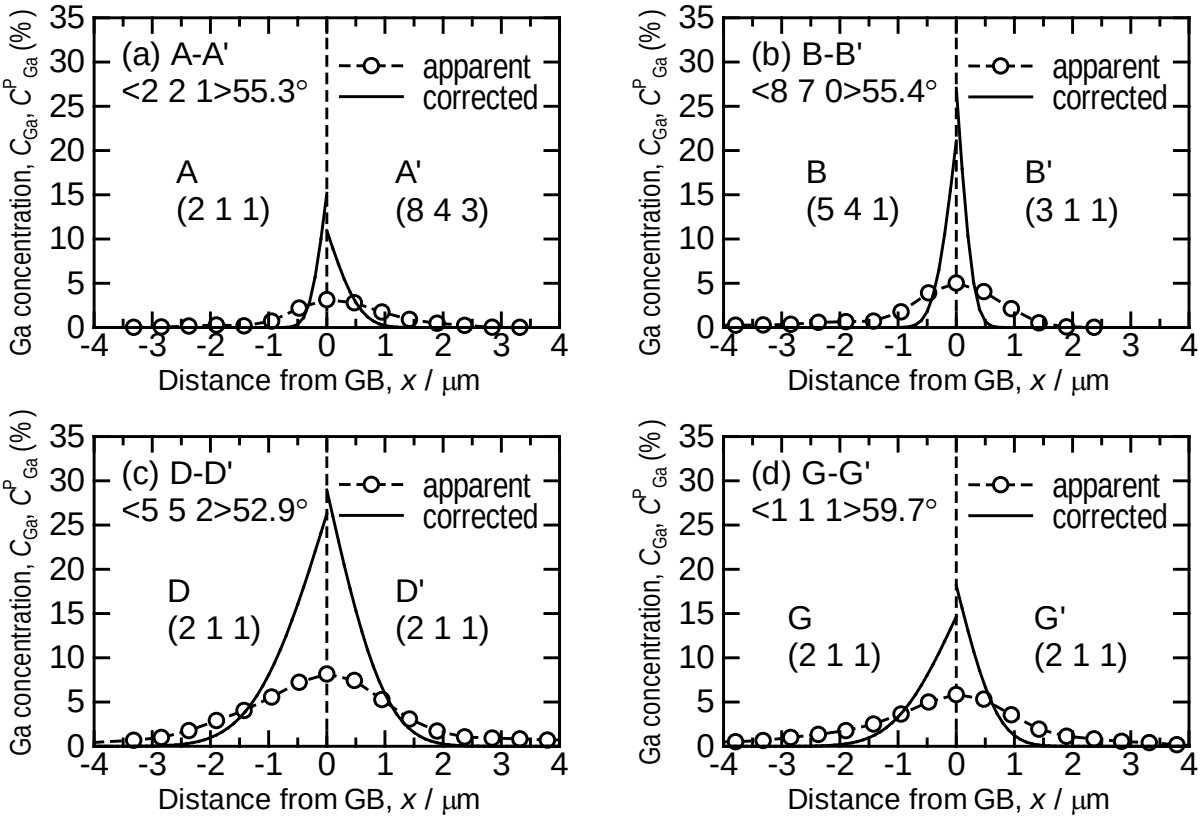

Figure 9 Apparent and corrected profiles of gallium concentration across GBs specified in Fig. 5. Parameters which represent GB structures are included.

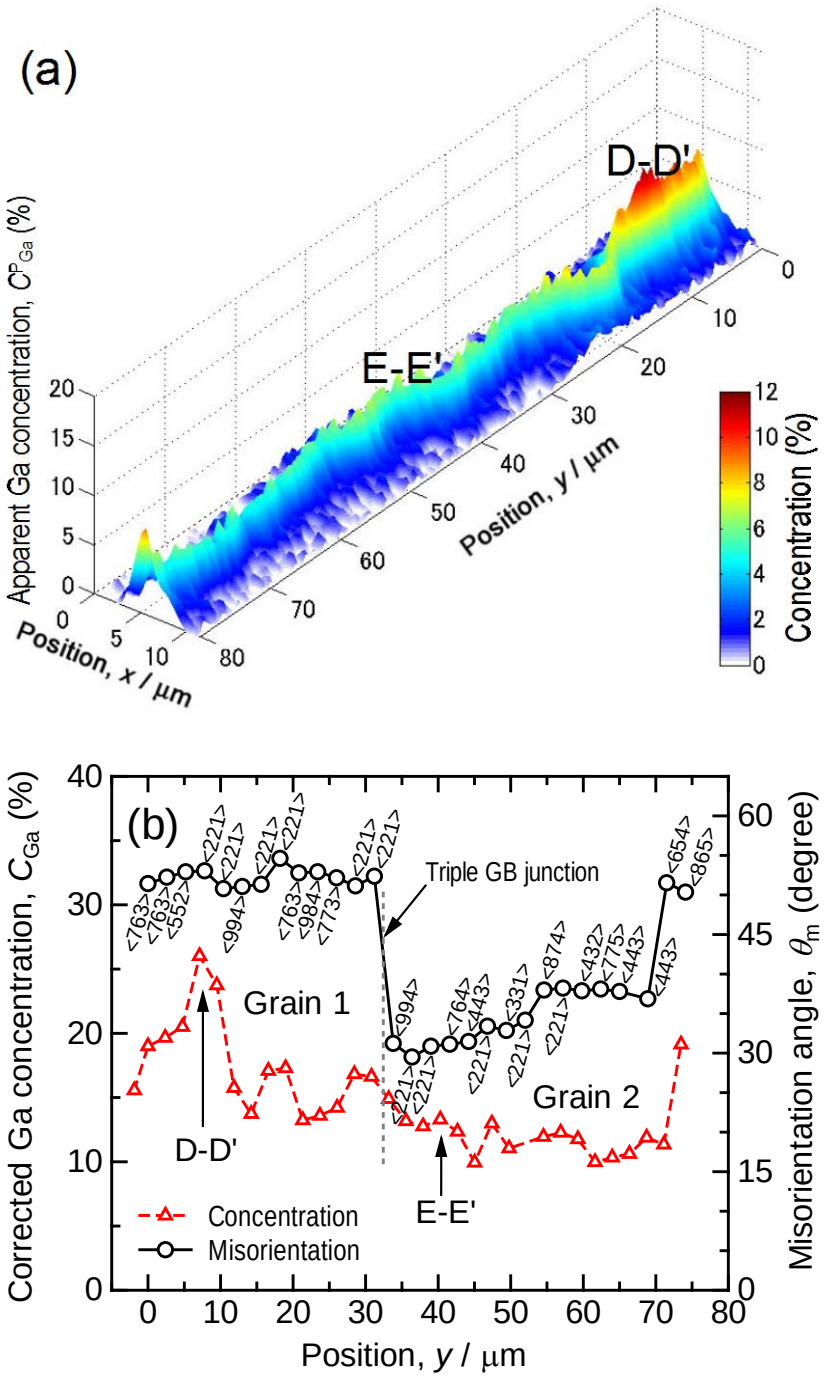

Figure 10 Changes in gallium concentration along GB, (a) corrected gallium concentration along the specific GB specified in Fig. 5 and (b) the variation of misorientation along and rotation axis along the same GB together with the gallium concentration variation.